Title
Analytic Prediction of Rotor Broadband Noise with Serrated Trailing Edges

Journal
78th Vertical Flight Society Annual Forum and Technology Display Forum 2022

Authors
Li, S
Lee, S

Publication Date
2022

Analytic Prediction of Rotor Broadband Noise with Serrated Trailing Edges

Sicheng (Kevin) Li
Ph.D. Candidate

Seongkyu Lee
Associate Professor

Department of Mechanical and Aerospace Engineering
University of California, Davis
Davis, California, 95616 U.S.A.

ABSTRACT

Trailing-edge serrations are known to be an effective way to reduce broadband noise on wing sections, but their noise reduction capabilities on rotorcraft have not been fully understood. This paper develops a new approach to analytically predicting and investigating broadband noise of rotors with serrated trailing edges. To achieve rotorcraft broadband noise predictions, we extend Lyu and Ayton's semi-infinite serrated wing model to include the finite blade span, the modified scattering coefficient, and the spanwise observer distance. The validations show good agreements with experimental data for serrated trailing-edge noise of a wing section, a hovering rotor, and a forward-flight rotor. Next, the effects of serration parameters on rotor broadband noise are studied. For optimal and realistic rotor broadband noise reduction, the desirable design of a serrated-blade rotor has the serration height to wavelength ratio of 2, the radial range of serrations from 50% blade span to the tip. It is also found that the sine-wave, chopped peak, or saw-tooth serration shapes reduce noise most among various shapes that are considered. Finally, noise reduction with serrations is applied to urban air mobility (UAM) aircraft. A 6-passenger eVTOL quadrotor is found to have more than 9 dB noise reduction potential with serrated trailing edges, where higher noise reductions are observed with higher tip speeds and fewer blades. Serrated-blade quadrotors are found to have the dipole broadband noise directivity, and noise reductions are observed at all observer angles.

NOTATION

c	chord length, m
c_0	speed of sound, m/s
E_n	serration shape coefficient
f	frequency, Hz
$F(\eta)$	serration geometry function
$2h$	serration height, m
k	acoustic wavenumber, ω/c_0
k_x	aerodynamic wavenumber, ω/V_c
k_y	spanwise wavenumber, ky/S_0
l	serration wavelength, m
l_y	spanwise turbulence lengthscale, $1.6V_c/\omega$, m
L	effective lift function, N/m
M	blade sectional flow Mach number
N_b	number of blades
N_r	number of rotors
n	mode number
OASPL	overall sound pressure level, dB
R	rotor radius, m
r	span radial location, m
r_o	observer distance, m
RPM	revolution per minute
S_{pp}	acoustic PSD, $\mathrm{Pa}^2/\mathrm{Hz}$
SPL	sound pressure level, dB
V_∞	blade sectional freestream velocity, m/s
V_c	convection velocity, $0.7V$, m/s
V_{tip}	rotor tip speed, m/s
$\vec{x}$	observer position, m
X,Y,Z	coordinates in airfoil section frame, m
X_2,Y_2,Z_2	observer global coordinate, m
α	angle of attack, deg
α_{sh}	rotor shaft angle of attack, deg
μ	rotor advance ratio
Δr	blade section span, m
ω	angular frequency, rad/s
Φ_{pp}	surface pressure spectrum, $\mathrm{Pa}^2/\mathrm{Hz}$
ϕ_o	observer elevation angle, deg
ψ_o	observer azimuth angle, deg
θ_o	observer angle to the trailing edge, deg

Presented at the Vertical Flight Society 78th Annual Forum & Technology Display, Fort Worth, Texas, USA, May 10-12, 2022.

INTRODUCTION

Noise is one of the top concerns in rotorcraft applications. For conventional helicopters, the operating noise level is limited by the regulations (Ref. 1). For urban air mobility (UAM) aircraft, noise is a major barrier that hinders a successful market due to its public nonacceptance (Ref. 2). The UAM companies are devoted to reduce noise of their aircraft (Refs. 3, 4, 5). The community noise of rotorcraft is mainly contributed by the aerodynamic noise generated by the rotor blades, categorized as tonal noise and broadband noise. Rotor tonal noise, including high-speed impulsive noise(Ref. 6) and blade vortex interaction (BVI) noise (Ref. 7), is important for in-plane and long-distance observers. Rotor broadband noise, including blade-wake-interaction (BWI) noise (Ref. 8) and airfoil-self noise (Ref. 9), is important for out-of-plane observers, and it is in the sensitive frequency range of human hearing. During forward and hovering flights, where blade wake interactions are weak, airfoil-self noise is the main broadband noise source (Ref. 10).

The vehicle operation and the rotor design can be used to achieve rotorcraft noise reductions. During a rotorcraft operation, noise can be reduced by adjusting the flight path and vehicle attitude (Refs. 11, 12, 13), including increasing the flight altitude, avoiding populated areas, and decreasing the descending flight angle. On the other hand, noise reduction concepts can be incorporated into the rotorcraft design phase. The rotor tip speed and the number of blades can be varied to reduce tonal and broadband noise (Refs. 14, 15, 16). The tail rotor noise can be eliminated by the No Tail Rotor-style (NOTAR) tailboom system (Ref. 17). Swept and tapered blades at the rotor tip are widely adopted to reduce the BVI noise (Refs. 18, 19). In addition, turbulent boundary layer trailing-edge broadband noise (Ref. 20) can be attenuated by turbulent hydrodynamic energy reduction or acoustic scattering modification. These modifications include active flow controls (Ref. 21), finlets (Ref. 22), porous material (Ref. 23), acoustics liners (Ref. 24), and edge serrations (Ref. 25).

Serrated blades are preferred among the aforementioned broadband noise reduction techniques on vertical flight rotors. The serrations are easy to manufacture, and the rotor performance remains unchanged after adding the serrated edges (Ref. 26). Regarding the mechanism of the noise reduction, on properly designed serrations, destructive interference can be achieved between the serration root and tip, and the acoustic energy is redistributed to the high cut-off modes (Ref. 25). Although serrations have been widely used on wind turbines to reduce trailing-edge noise (Ref. 27), the application of this idea to vertical flight rotors is still limited. The drone rotors with serrated trailing edges are experimentally shown to have noise reductions at high frequencies (Refs. 28, 29). However, rapid design tools with proper analytical models to investigate the potential to reduce rotor broadband noise are still lacking. Therefore, this paper will focus on the analytical predictions of rotor broadband noise reduction with serrated trailing edges.

The early work of Howe used the tailored Green's function to theoretically predict trailing-edge noise of the serrated blade (Ref. 30), but this method was shown to over-predict the noise reduction (Ref. 31). Using the Schwarzschild method (Ref. 32) and the Wiener-Hopf method (Ref. 33), Lyu et al. (Ref. 31) and Huang (Ref. 34) derived more recent serrated trailing-edge noise models, respectively. However, these two models cannot be solved exactly and require extensive computational time for the entire rotor blade. Using the Wiener-Hopf method, Ayton (Ref. 25) developed a new model that can be solved exactly with an infinite number of the scattering modes, where any serrated shape can be expressed in a 2-D function. To further reduce the computational cost, Lyu and Ayton (Ref. 35) simplified Ayton's model (Ref. 25) by implementing a finite number of cut-on and cut-off modes.

In this paper, Lyu and Ayton's model (Ref. 35) will be used to predict trailing-edge noise from the serrated rotor. This model requires the wall pressure fluctuations upstream of the trailing edge, which can be obtained from Lee's wall pressure spectrum model (Ref. 36), which is suitable for adverse pressure gradient flows. An underlying assumption in Lyu and Ayton's model is that the boundary layer formation upstream of a trailing edge is not affected by the appearance of the serration structures. This assumption was confirmed by Direct Numerical Simulation (DNS), showing that the wall pressure spectrum change upstream of a trailing edge is negligible with the addition of the serrations (Refs. 37, 38). The boundary layer parameters used to calculate the wall pressure spectrum are obtained from the low-fidelity XFOIL panel method (Ref. 39), where the two-equation boundary layer formations are used to calculate a turbulent boundary layer flow around an airfoil surface. As for the rotor aerodynamics, the hovering flight is solved using the blade element momentum theory (BEMT), while the forward flight is solved by coupling the blade element theory (BET), Peters-He dynamic inflow model (Ref. 40), and the moment-balance trim solution (Ref. 41).

The current study will extend the capabilities of the rotorcraft broadband noise prediction tool, UCD-QuietFly (Ref. 42), from a straight trailing edge to a serrated trailing edge. For the straight blade sections, Amiet's model (Ref. 43) is transformed into the rotor blade coordinates (Ref. 44) to predict trailing-edge noise. Amiet's model uses the Schwarzschild method (Ref. 32) to solve an acoustic scattering problem by a trailing edge (Ref. 45). For the serrated sections, Lyu and Ayton's model is used. Note that a user-defined blade geometry accepts a blend of straight and serrated shapes on a rotor blade.

We will first validate this developed toolchain for serrated wing sections and serrated rotor blades against existing experimental data. Second, the importance and mechanism of serrated trailing edges used on rotorcraft will be addressed. Third, various parameters including serration number, shapes, and locations will be compared for their broadband noise reductions capabilities. Finally, a quadrotor conceptual air taxi aircraft will be used to demonstrate the effectiveness of noise reduction with trailing-edge serrations in the context of urban air mobility operations.

METHOD AND FORMULATION

The straight blade sections are calculated using Amiet's trailing-edge model (Ref. 43) improved by Roger and Moreau (Ref. 46), which reads as

$$S_{pp}(\vec{x},\omega) = \left(\frac{kcZ}{4\pi S_0^2}\right)^2 2\Delta r|\mathbf{L}|^2\Phi_{pp}(\omega)l_y(\omega,k_y) \qquad (1)$$

where $S_0^2 = X^2 + \beta^2 \left(Y^2 + Z^2\right)$, $\beta^2 = 1 - M^2$, k is the acoustic wavenumber, c is the chord length, Δr is the blade sectional span, L is the loading term, and Φ_{pp} is the wall pressure spectrum (Ref. 36). Equation (1) includes a factor of 4 compared to the original Amiet model since the scattering on one surface influences both surfaces of an airfoil section - a factor of 2 in the scattered acoustic pressure.

The spanwise correction length of the wall pressure spectrum is calculated using Corcos's model (Ref. 47) as

$$l_y(\omega, k_y) = \frac{\omega/(V_c b_c)}{k_y^2 + \omega^2/(V_c b_c)^2} \tag{2}$$

where b_c is a constant taken as 1.6 in this paper.

The loading term L includes the contributions from the trailing-edge scattering L_1 and the leading-edge back-scattering L_2, such that $L = L_1 + L_2$. We have added a correction term in L_1, which is the last term in Eq. (3) in order to ensure that a factor of 4 that was described earlier is only applied to the scattering part, but not to the incident part (Ref. 48).

$$L_1 = -\frac{e^{2iC}}{iC}\Bigg\{(1+i)e^{-2iC}\sqrt{\frac{B}{B-C}}E^*[2(B-C)] - (1+i)E^*[2B] + 1 - e^{-2iC} + \frac{e^{-2iC}}{4}\Bigg\} \tag{3}$$

$$B = \bar{K}_x + M\bar{\mu} + \bar{\kappa} \tag{4}$$

$$C = \bar{K}_x - \bar{\mu}(X/S_0 - M) \tag{5}$$

For straight blades, The Roger and Moreau's leading-edge back-scattering correction (Ref. 46) is given in Eq. (6). This term is important for small chord lengths and low frequencies, where the reduced wavenumber kc is small.

$$\frac{1}{H}L_2 = \left\{e^{4i\bar{\kappa}}[1-(1+i)E^*(4\bar{\kappa})]\right\}^c - e^{2iD} + i[D + k_x^* + M\bar{\mu} - \bar{\kappa}]G \tag{6}$$

where

$$H = \frac{(1+i)e^{-4i\bar{\kappa}}(i - \Theta^2)}{2\sqrt{\pi}(\alpha-1)k_x^*\sqrt{B}} \tag{7}$$

$$D = \bar{\kappa} - \bar{\mu}X/S_0; \quad \alpha = V_\infty/V_c \tag{8}$$

$$\Theta = \sqrt{\frac{\bar{K}_x + \bar{\mu}M + \bar{\kappa}}{k_x^* + \bar{\mu}M + \bar{\kappa}}} \tag{9}$$

$$G = (1+\varepsilon)e^{i(2\bar{\kappa}+D)}\frac{\sin D - 2\bar{\kappa}}{D - 2\bar{\kappa}} + (1-\varepsilon)e^{i(-2\bar{\kappa}+D)}\frac{\sin D + 2\bar{\kappa}}{D+2\bar{\kappa}} + \frac{(1+\varepsilon)(1-i)}{2(D-2\bar{\kappa})}e^{4i\bar{\kappa}}E^*(4\bar{\kappa}) - \frac{(1-\varepsilon)(1+i)}{2(D+2\bar{\kappa})}e^{-4i\bar{\kappa}}E^*(4\bar{\kappa}) + \frac{e^{2iD}}{2}\sqrt{\frac{2\bar{\kappa}}{D}}E^*(2D)\left[\frac{(1+i)(1-\varepsilon)}{D+2\bar{\kappa}} - \frac{(1-i)(1+\varepsilon)}{D-2\bar{\kappa}}\right] \tag{10}$$

and the imaginary part of $\{\}^c$ in Eq. (6) is multiplied by $\varepsilon = (\sqrt{1+1/(4\bar{\mu})})^{-1}$.

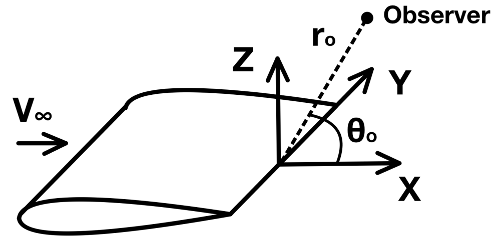

Fig. 1: Observer distance and angle in the blade local coordinates.

For the serrated blade sections, the original Lyu and Ayton model (Ref. 35) reads

$$S_{pp} \approx \frac{\bar{k}}{2\pi r_o}\sin^2\frac{\theta_o}{2}\frac{\chi + \bar{k}}{2\left(\chi - \bar{k}\cos\theta_o\right)^2}\sum_{n=-\infty}^{+\infty}\Pi(\omega, k_y)|E_n(\lambda)|^2 \tag{11}$$

where the observer location, in terms of r_o and θ_o are shown in Fig. 1. The observer angle, θ_o, is defined in the $X - Z$ plane, and the spanwise location is not considered in the original model.

We propose corrections to this equation to implement Lyu and Ayton's model in rotor cases. First, the limitation of this model is the assumption of the unit span length, and the blade section span length, Δr, should be multiplied in Eq. (11). Second, to match the attenuation rate of the acoustic propagation, Eq. (11) is divided by the observer distance, r_o. Third, the effect of the spanwise observer location is included in $r_o^2 = (x/\beta)^2 + y^2 + z^2$ as well as in the spanwise wavenumber, such that $k_y = 2\pi n/l + ky/S_0$. In the original model, r_o^2 and k_y were defined as $(x/\beta)^2 + z^2$ and $2\pi n/l$, respectively (Ref. 35). Fourth, a factor of four is added to correct the scattering effect on the upper and lower surfaces, which is similar to Eq. (1). The new equation used in this paper is given as

$$S_{pp} \approx \frac{4\Delta r\bar{k}}{2\pi r_o^2}\sin^2\frac{\theta_o}{2}\frac{\chi + \bar{k}}{2\left(\chi - \bar{k}\cos\theta_o\right)^2}\sum_{n=-\infty}^{+\infty}\Pi(\omega, k_y)|E_n(\lambda)|^2 \tag{12}$$

where the wavenumber-frequency wall pressure spectrum is

$$\Pi(\omega, k_y) = \frac{1}{\pi}\Phi_{pp}(\omega)l_y(\omega, k_y) \tag{13}$$

$\bar{k} = k\beta$ is the the mean-flow-corrected acoustic wavenumber; θ_o the observer angle; $\chi = \bar{k}_x\beta$ the corrected convective wavenumber; $\bar{k}_x = k_x + kM/\beta^2$ and $\lambda = (\bar{k}_x - \bar{k}\cos\theta)\bar{c}/4$ are the inputs to the radiation function $E_n(\lambda)$ (Ref. 49); $\bar{c} = 2h/\beta$ the corrected serration amplitude. Note that the fundamental mode of $n = 0$ is the most important modal term, and the effects of the higher modes appear when $k/\beta > 2n\pi$.

$$E_n(\lambda) = \int_0^1 e^{i\bar{c}F(\eta)(\bar{k}_x+\lambda)} e^{-i2\pi n\eta} d\eta \tag{14}$$

The radiation function of the serrated geometry is given in Eq. (14), where $F(\eta)$ is the non-dimensional height of the serrations, η is zero at the root and one at the tip of a blade section. We use $2h$ and l to denote the dimensional peak-to-peak amplitude of the serration and the serration wavelength, respectively, for future usages in the paper, as shown in Fig. 3. This function provides the flexibility to describe arbitrary serration geometries, including a blend of straight and serrated trailing edges.

The selected trailing-edge serrated geometries are plotted in Fig. 2, where their corresponding equations are given in Eq. (15). The geometry equations describe the serration height $F(\eta)$ as a function of the η coordinate within a wavelength of l, where the origin of the $F - \eta$ coordinate is located at the lower-left corner.

In UCD-QuietFly, the starting blade radial location and shape of the serration can be customized, as shown in Fig. 3. Although a straight blade can be calculated in Lyu and Ayton's model, Amiet's trailing-edge noise model is much faster when used on straight sections. In the current study, a rotor blade is segmented into 40 sections of equal length. The rotor design and operational parameters, such as the collective and cyclic pitch, blade twist, forward speed, multi-rotor hub locations, etc., are included in the blade section coordinate transformations (Ref. 44). For the current calculations of trailing-edge serrations in UCD-QuietFly, the serration geometries are attached to the rotor blade edges instead of cut-in.

In the current study, the boundary layer parameters are calculated using the XFOIL panel method code (Ref. 39), the wall pressure spectrum near the blade trailing edge using Lee's model (Ref. 36), the hovering flights using blade element momentum theory (BEMT), the forward flights using an in-house low-fidelity rotor comprehensive code (Ref. 50), and trailing-edge noise using UCD-QuietFly (Refs. 44,42,51,52).

Table 1: Airfoil Section Validation Parameters

Parameters	Verification (Fig. 4)	Validation (Fig. 5)
Wing	NACA 0012	NACA 0018
V_∞ (m/s)	241	34
α (deg)	1.8	0.0
c (m)	0.2	0.2
Δr (m)	0.15	0.4
r_o (m)	1 & 13	1.0548
θ_o (deg)	90	90

$$F_{Saw-tooth} = \begin{cases} 2\eta - 0.5, & 0 < \eta < 0.5 \\ 1.5 - 2\eta, & 0.5 < \eta < 1 \end{cases} \tag{15a}$$

$$F_{Square} = \begin{cases} 0.5, & 0 < \eta < 0.25 \\ -0.5, & 0.25 < \eta < 0.75 \\ 0.5, & 0.75 < \eta < 1 \end{cases} \tag{15b}$$

$$F_{Sine} = 0.5\sin 2\pi\eta, \quad 0 < \eta < 1 \tag{15c}$$

$$F_{Half-sine} = 0.5\sin \pi\eta, \quad 0 < \eta < 1 \tag{15d}$$

$$F_{Ogee} = \begin{cases} 4\eta - 0.5 - \sin\pi\eta, & 0 < \eta < 0.5 \\ 3.5 - 4\eta) - \sin\pi\eta, & 0.5 < \eta < 1 \end{cases} \tag{15e}$$

$$F_{Chopped\ peak} = \begin{cases} 10/3\eta, & 0 < \eta < 0.15 \\ 0.5, & 0.15 < \eta < 0.35 \\ 11/8 - 5/2\eta, & 0.35 < \eta < 0.75 \\ 2\eta - 2, & 0.75 < \eta < 1 \end{cases} \tag{15f}$$

$$F_{Slitted\ U-root} = \begin{cases} 2\eta, & 0 < \eta < 0.25 \\ 0.94 - 1.78\eta, & 0.25 < \eta < 0.7 \\ 2.5 - 4\eta, & 0.7 < \eta < 0.75 \\ -3.5 + 4\eta, & 0.75 < \eta < 0.8 \\ -1.5 + 1.5\eta, & 0.8 < \eta < 1 \end{cases} \tag{15g}$$

$$F_{Slitted\ U-root} = \begin{cases} 2\eta, & 0 < \eta < 0.25 \\ 0.94 - 1.78\eta, & 0.25 < \eta < 0.7 \\ -0.5, & 0.7 < \eta < 0.8 \\ -1.5 + 1.5\eta, & 0.8 < \eta < 1 \end{cases} \tag{15h}$$

VALIDATIONS

This section first compares Amiet's model (Ref. 43) and the modified Lyu and Ayton's model (Ref. 35) on the calculations of trailing-edge noise on the straight wing section. The prediction of noise reduction on a serrated wing section is validated against the experiment. Second, broadband noise of two serrated-blade rotors, one in hovering flight and the other in forward flight, is calculated in UCD-QuietFly and validated against the experiments.

Serrated Wing Section

This section verifies the implementation of the modified Lyu and Ayton's model against Amiet's model and validates the noise reduction with serrated trailing edges against experimental data. Table 1 shows the verification and validation cases. The first validation case is given in Fig. 4, where the modified Lyu and Ayton's model is used to predict trailing-edge noise of a straight wing section, which is compared to the results of Amiet's model. The overlapping of these two models demonstrates the correctness of our improvements shown in Eq. (12).

The predictions of trailing-edge noise of a serrated wing and a straight wing are provided in Fig. 5, where the experiment data is given (Ref. 53). The noise reduction, ΔSPL (sound pressure level), is the Decibel difference between a straight

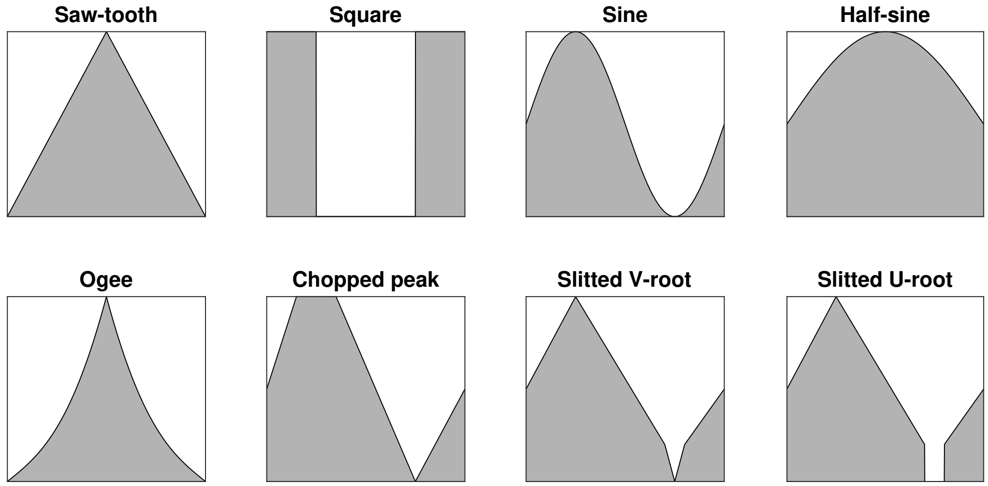

Fig. 2: Trailing-edge serrated geometries. The $\eta - F$ serration coordinate has the origin at the lower-left corner, with the serration wavelength of l.

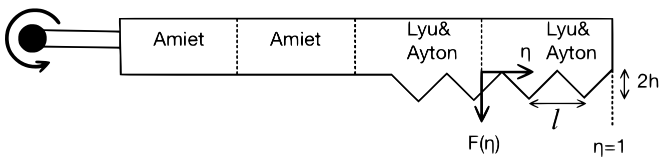

Fig. 3: Serrated rotor blade geometry.

blade and a serrated blade in the same conditions. Amiet's model was used on the straight blade, while Lyu and Ayton's model was used on the serrated blade in this validation study. It is seen that the noise reduction is predicted well at middle frequencies. The over-predictions of the noise reduction are observed in the high-frequency range, which is likely due to other noise sources in the experiment that are not included in the current acoustic model, such as misaligned small vortical flows at the serration root sections (Ref. 54). The existence of these additional sources is case-dependent.

Table 2: Hovering Rotor Validation Parameters

Parameters	APC Slow Flyer 11X4.7
R (m)	0.14
N_b	2
RPM	3000
Airfoil	E63(hub)/ClarkY(tip)
ϕ_o (deg)	90
r_o (m)	1.65
Shape	Sawtooth
$2h$ (m)	0.006
l (m)	0.00322
serration r/R range	0.5-1.0

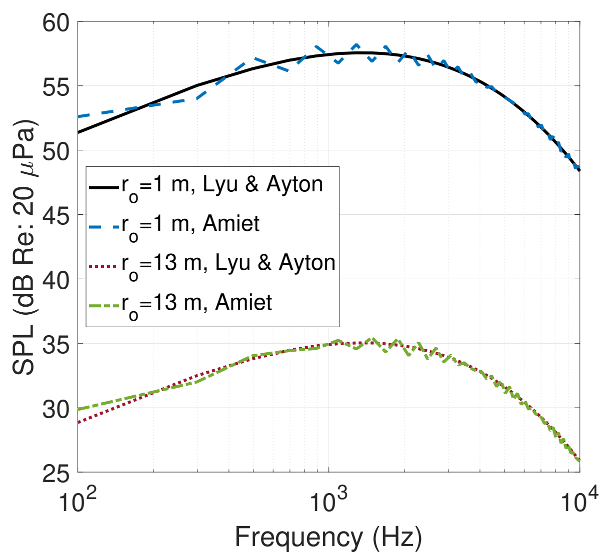

Fig. 4: Comparison of Amiet's model and Lyu and Ayton's model on a straight wing section at different observer distances.

Serrated Rotor

A hovering rotor validation case is provided in Table 2, where an APC drone rotor is serrated from the mid-span to the tip. The experiment of a hovering rotor was conducted in an acoustic wind tunnel (Ref. 28). The microphone is 1.65 m directly above the rotor hub. The predictions of the rotor noise with straight and serrated trailing edges are given in Fig. 6. The predictions of the straight-blade rotor noise match the experiment very well. At the middle to high frequencies, the predictions of the serrated rotor noise give reasonable noise reductions compared to the experiment, while some under-predictions appear. In the low-frequency range, the serrated-rotor broadband noise is over-predicted, due to the limitation of Lyu and Ayton's model in a small chord length. We found that blades with chord lengths larger than 0.1 m do not have this over-prediction issue at low frequencies. Overall, although the serrated trailing-edge noise predictions are not perfect compared to the experiment, they give reasonable predictions in noise reduction.

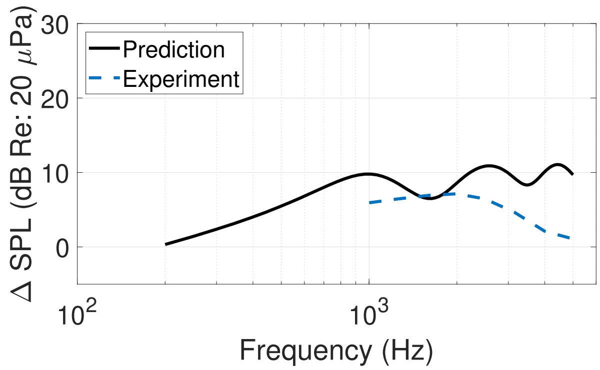

Fig. 5: Noise reduction validation of the serrated trailing-edge noise model on the wing section. The serration shape is saw-tooth, $2h = 0.04$ m, and $l = 0.02$ m. Experiment data is given in Ref. 53

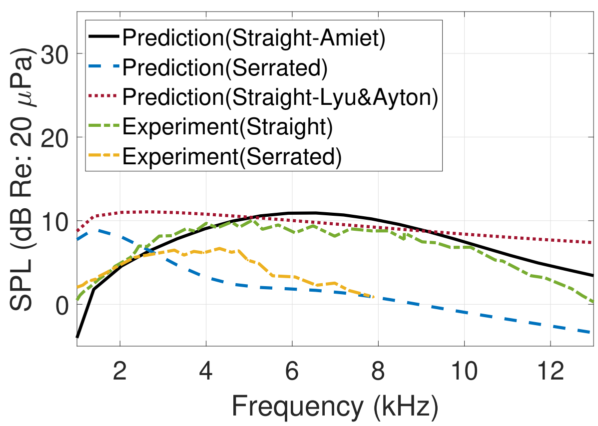

Fig. 6: Validation of UCD-QuietFly on the serrated drone rotor. Experiment data is given in Ref. 28, with broadband components extracted.

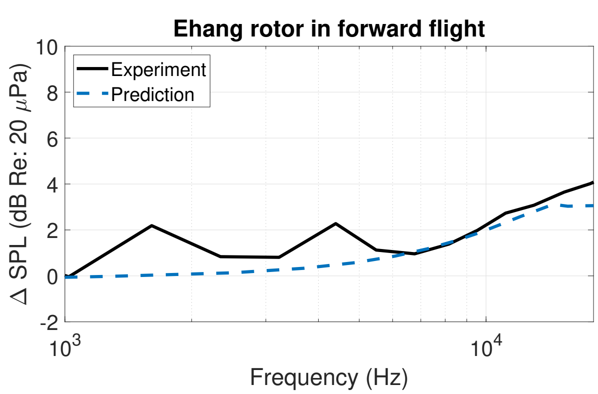

Fig. 7: Validation of UCD-QuietFly on the serrated drone rotor in forward flight. Experiment data is given in Ref. 29, with broadband components extracted.

In addition to the broadband noise validation of a hovering rotor, broadband noise is predicted on a forward-flight eHANG rotor with serrated trailing edges. The eHANG drone rotor parameters are provided in Table. 3, where the acoustic measurements were taken in an anechoic wind tunnel (Ref. 29).

Table 3: Forward Rotor Validation Parameters

Parameters	eHANG Ghost 3.0
R (m)	0.13
N_b	2
RPM	7200
μ	0.1931
α_{sh} (deg)	15
Airfoil	A18
ϕ_o (deg)	-56.31
ψ_o (deg)	180
r_o (m)	1.49
Shape	Saw-tooth
$2h$ (m)	0.00326
l (m)	0.00652
serration r/R range	0.2-1.0

The microphone is in the forward direction of the rotor, with an elevation angle of -56.31 °, azimuthal angle of 180 °, and a distance of 1.49 m. The tested rotor has saw-tooth serrations with a height to wavelength ratio, $2h/l$, of 0.5. The noise reduction between a serrated-blade rotor and a straight-blade rotor is predicted in Fig. 7 and compared against the experimental data. It is seen that the prediction has good agreement with the measurements, especially above 5 kHz, where apparent noise reductions are present.

RESULTS

First, the serration effects on rotor broadband noise are assessed by varying the trailing-edge serration parameters: number of serrations, serrations' starting radial location, serration geometry, serration height, and tip-to-root height ratio. Next, the trailing-edge serrations are applied to NASA's UAM eVTOL quadcopter designs with varying tip speeds and blade numbers. The directivity of the serrated-blade quadrotor in hover is compared to the quadrotor with straight blades.

Effects of Serration Parameters

The baseline rotor case is an APC Slow Flyer drone rotor with serrated trailing edges, whose parameters are given in Table. 2. For each parameter studied, other parameters are kept as the baseline values. In this parameter study, the straight-blade rotor noise prediction is used as a reference, which is calculated using Lyu and Ayton's model from the corresponding serration region outboard, and using Amiet's model inboard. The purpose of this practice is to reduce computational time using the faster Amiet's model for the inboard sections, which are are less important acoustically. The noise difference between the straight-blade rotor and serrated-blade rotor (ΔOASPL) is calculated. Note that we use Lyu and Ayton's model even for the straight blade at the outboard sections where the serrations would be located so that the noise comparison between the straight blade and the serrated blade is fair. The frequency range of summation for the OASPL (overall sound pressure level) is 0.1-13 kHz.

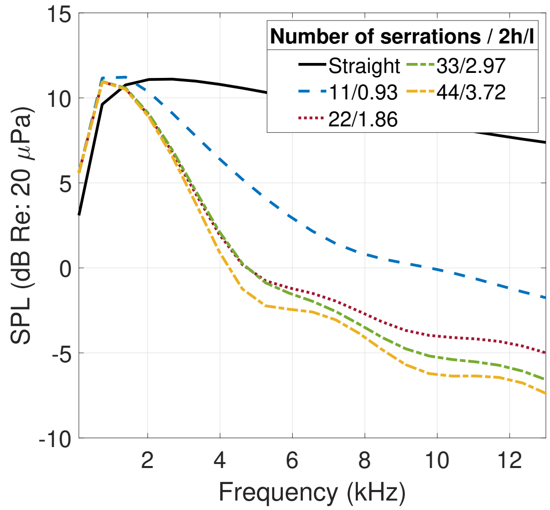

(a)

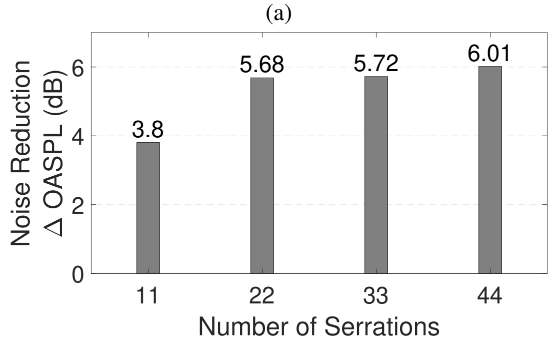

(b)

Fig. 8: The effect of the number of serrations on rotor broadband noise: (a) sound pressure level spectrum and (b) noise reduction compared to the straight-blade rotor.

The effect of varying the number of serrations is shown in Fig. 8, where the rotor trailing edges have saw-tooth serrations from its 50 % radial position to the tip. As the number of serrations increases, the serration wavelength is shortened, which can also be seen as the effect of changing the serration wavelength. The frequency spectrum of SPL in Fig. 8(a) shows that noise reductions occur in the mid- to high-frequency range (above 2.5 kHz), while noise increases are seen in the low frequencies. Increasing the number of serrations (or reducing the serration wavelength) reduces the noise level. However, as more serration shapes are added, the effectiveness of noise reduction is reduced. With more serrations or the shorter wavelength, the destructive interference on the rotor blade is increased, since the modal coefficient in Eq. (14) gets more oscillations with more serrations on the blade span. Therefore, considering the manufacturing and structural challenges, 22 serrations ($2h/l$=2) are desirable although more serrations slightly improve the noise reduction.

Figure 9 shows the effects of changing the starting radial position of the serrations, where the inboard of the starting position has straight edges, as shown in Fig. 3. The frequency spectrum indicates that the noise levels at the mid and high frequencies (above 2 kHz) are reduced with the increasing span portion of the serrated blade, while the low-frequency

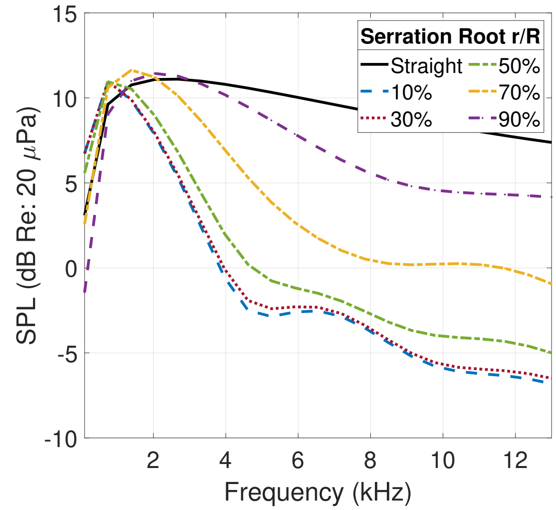

(a)

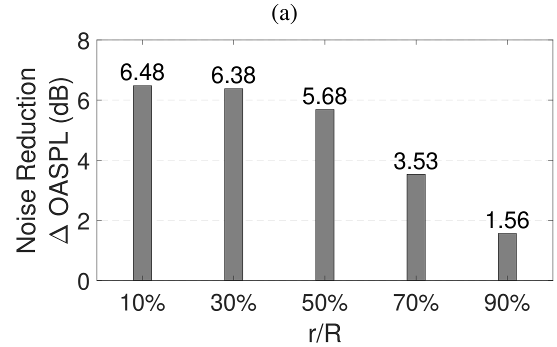

(b)

Fig. 9: The effect of starting radial locations of the serrations on rotor broadband noise: (a) sound pressure level spectrum and (b) overall sound pressure level reduction compared to the straight-blade rotor.

range has a slight noise increase. This noise increase might result from the model difference when blending Amiet's model and Lyu and Ayton's model on the same blade, where some discrepancies at the low frequencies are present in Fig. 6. The benefit benefit of using Amiet's model for the straight portion of a blade is to reduce the computational time. The trend of the noise reduction shows that the noise level of the serrated rotor keeps decreasing as the starting position of the serrations moves to the root, but the tip serrations are more effective in reducing noise, since the higher flow speeds at the tip sections give the higher noise levels. The most outboard 10% sections provide a noise reduction of 1.56 dB, and the 70-90% and the 50-70% sections each provide noise reductions of about 2 dB. However, the 30-50% sections give a noise reduction of less than 1 dB, and the inboard 30% sections have minimal noise reduction benefits. Thus, it is suggested that using trailing-edge serrations starting from 50% r/R is preferred.

Figure 10 demonstrates the effect of increasing the serration height on broadband noise. The APC Slow Flyer rotor has a chord length of about 28 mm at 75% r/R, so attaching too large serration heights is unrealistic. Since the serrations are attached to the blade trailing edges, this approach results in increasing the blade chord length, and the impacts of vary-

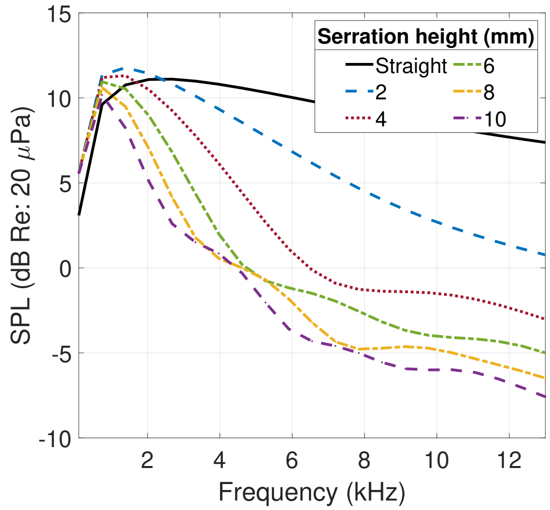

(a)

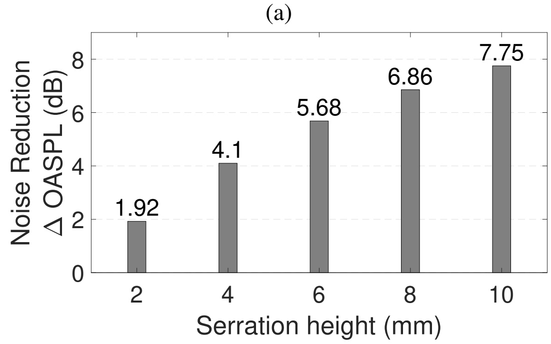

(b)

Fig. 10: The effect of serration heights on rotor broadband noise: (a) sound pressure level spectrum and (b) overall sound pressure level reduction compared to the straight-blade rotor.

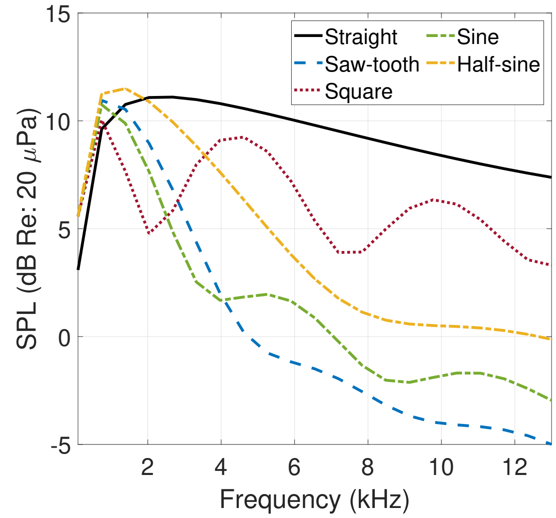

(a)

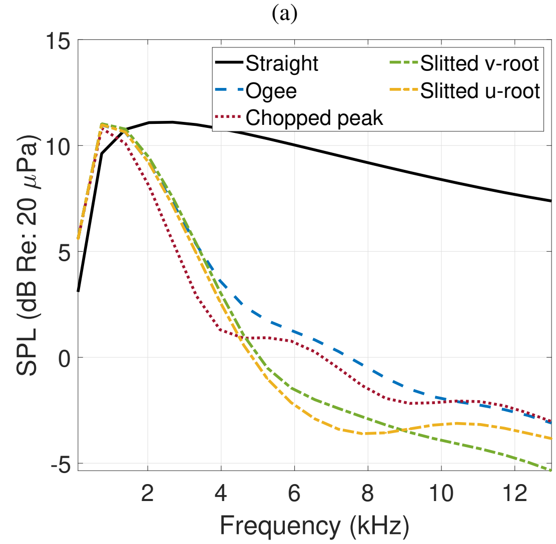

(b)

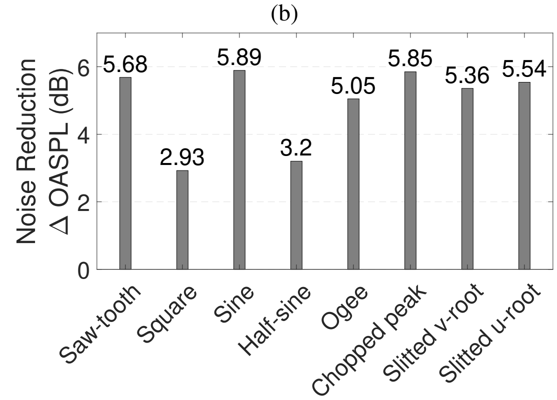

(c)

Fig. 11: The effect of serration shapes on rotor broadband noise: (a) (b) sound pressure level spectrum of the shapes in Eq. (15), and (c) overall sound pressure level reduction compared to the straight-blade rotor.

ing the chord length on the boundary layer condition are neglected in this study. It is observed that increasing the serration height has noticeable benefits of noise reduction, but this benefit is reduced at the larger serration heights. As the serration height increases, the incline angle between the serration and the blade span also increases to create stronger destructive interference between the serration tip and the root regions. The trend of changing the height to wavelength ratio $2h/l$ in Fig. 10 is the same as in Fig. 8; the higher $2h/l$ increases the noise reduction in a decreasing rate. In addition, more acoustic energy is redistributed to the higher-frequency cut-off modes (imaginary part of E_n) since the shape coefficient in Eq. 14 is a function of $k\bar{c} = 2kh/\beta$, which is proportional to the serration height.

The different serration shapes shown in Fig. 2 and Eq. (15) are used on the rotor to study their noise reduction capabilities. Figure 11 shows that the sine-wave shape gives the largest noise reduction, and the chopped peak and the saw-tooth shapes give similarly excellent noise reductions. The square and the half-sine shapes give the least noise reductions of about 3 dB. This trend is accounted for in the shape coefficient in Eq. (14), where the saw-tooth shape gives an increasing noise reduction as the frequency increases, but the square shape provides an up-and-down noise reduction behavior as a function of frequency. Note that the saw-tooth shape in Fig. 11(a) appears to have more noise reduction than the sine shape, specifically above 4 kHz. This trend is not reflected in the ΔOASPL plot, since the noise levels above 4 kHz for the saw-tooth and sine shapes are very small compared to the low-frequency noise.

For some rotor designs, different sizes of serrations may be preferred along the blade span. The effect of changing the serration height's tip-to-root ratio is given in Fig. 12. For the tip-to-root ratio of 0.5, the tip serration height is half of the starting r/R serration height, which is 0.5. The serration height linearly varies in between. The larger tip-to-root ratio creates a larger serration height at the tip to reduce noise. The tip-to-root ratio of 0.5 still provides a considerable noise reduction of 4.23 dB, although it is 1.45 dB lower than the constant geometries on the blade, as shown in Fig. 11(b). For tapered rotor blades with the reduced chord length at the tip, a smaller serration height at the tip region may be required for structural reasons.

Fig. 13: Conceptual design of an electric quadrotor (Ref. 16).

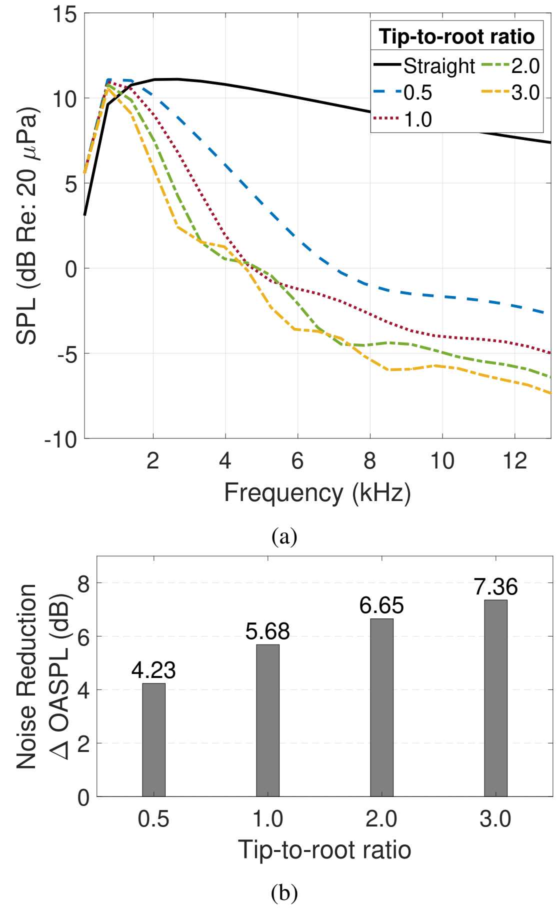

Fig. 12: The effect of starting radial locations of the serrations on rotor broadband noise: (a) sound pressure level spectrum and (b) overall sound pressure level reduction compared to the straight-blade rotor.

Table 4: UAM eVTOL Quadrotor Parameters (Ref. 16)

Parameters	6-passenger eVTOL quadrotor
R (m)	2.808
N_r	4
N_b	3/3/7
V_{tip} (m/s)	700/550/375
Airfoil	VR-12/SSC-A09
ϕ_o (deg)	-90
r_o (m)	150
Shape	Sawtooth
$2h$ (m)	0.0702
l (m)	0.0351
serration r/R range	0.5-1.0

Noise Reduction on an eVTOL Quadcopter

The UAM quadrotor conceptual designs shown in Fig. 13 are studied for their noise reduction potentials using trailing-edge serrations. The vehicle is operated in hovering condition, and the observer is 492 ft (150 m) directly below the quadrotor center. The detailed parameters of the vehicle can be found in Table. 4. In this study, the blade trailing edges of the quadrotor are serrated from mid-span to the tip with the saw-tooth geometry, whose serration height is $2h$=0.0702 m and serration wavelength is l=0.0351 m so that $2h/l$ becomes 2. For the straight-blade quadrotors, Amiet's model is used on the entire blade span. For reference, the blade chord length at 75% span is about 0.17 m. For this chord length, we found that Amiet's model and Lyu and Ayton's model provide almost the same results on the straight blade as demonstrated in Fig. 4. Thus, we have selected Amiet's model for its fast calculation. Three designs, with different tip speeds and numbers of blades, are studied in Fig. 14. The community background noise measured in a neighborhood in Sunnyvale, California (Ref. 55) is added in the figure as reference. The noise spectrum shows that the noise reductions appear in the entire frequency range. The Δ OASPL shows that the trailing-edge serrations have more noise reductions on the higher-tip-speed and fewer-blade designs. Trailing-edge serrations are effective in reducing noise in the mid-frequency range (1-5 kHz), which is masked by the community background noise. Although the high-frequency noise with serrations is not entirely masked by the background noise, the noise level even in the loudest condition is lower than 40 dB, which will help have the UAM aircraft much more favorably received by the public. In sum, using trailing-edge serrations as a noise reduction technique, multi-rotor eVTOL aircraft have the potential to reduce broadband noise by more than 9 dB as shown in Fig. 14(b), which is significant considering the unmasked eVTOL noise in the urban environment (Ref. 42).

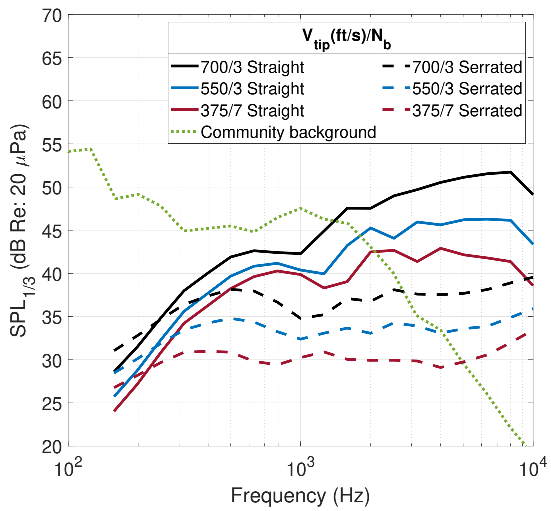

(a)

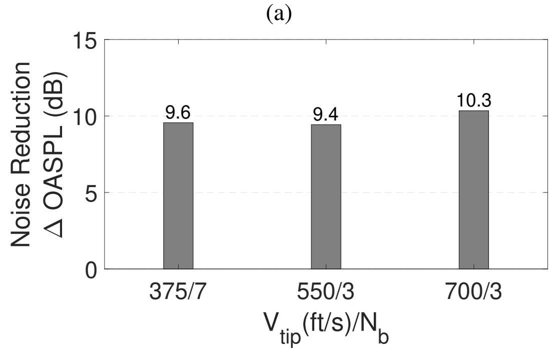

(b)

Fig. 14: Effects of using serrated blades on broadband noise of a eVTOL quadrotor, with various design tip speeds and numbers of blades. The observer is located at 492 ft directly underneath the vehicle. The serration height is 2h=0.0702 m and the serration wavelength is l=0.0351 m. The community background noise is given in Ref. 55. (a) sound pressure level spectrum and (b) overall sound pressure level reduction compared with the straight-blade rotor.

The hemispheric broadband noise directivities of the UAM eVTOL quadrotor are calculated in Fig. 15, including the straight-blade quadrotor, the serrated-blade quadrotor, and the noise reduction. The vehicle parameters are given in Table 4, and the radius of the observer hemisphere is 150 m. The quadrotor selected for this directivity study has three blades and the tip speed of 700 ft/s. The blue dot in Fig. 15 represents the vehicle position. The straight-blade quadrotor noise is calculated using Amiet's model. It is seen that both the straight-blade and the serrated-blade quadrotors have dipole directivity, where the highest noise level is found directly below the quadrotor. The noise reduction is observed for all observer locations on the hemisphere, except for the very small elevation angles (in-plane) due to the model difference at low frequencies. This directivity pattern on serrated-blade rotorcraft is consistent with the directivity on a serrated airfoil section, where noise reductions are observed for all observer angles (Refs. 56,25).

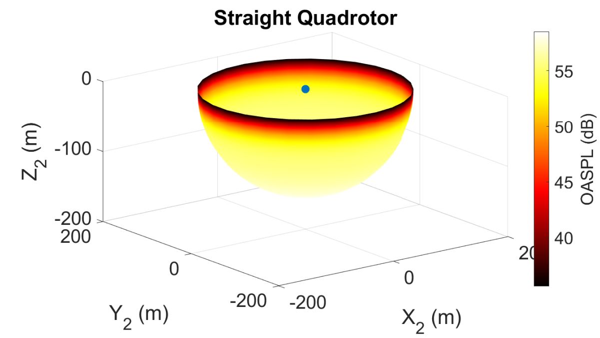

(a)

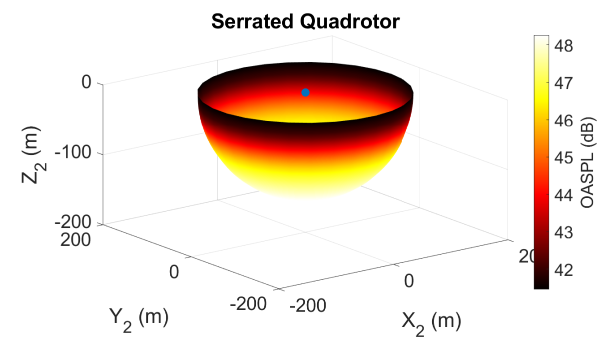

(b)

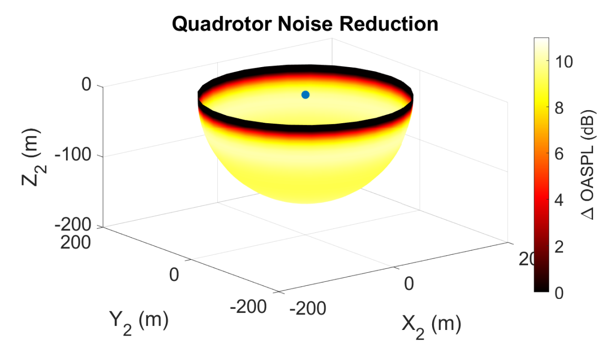

(c)

Fig. 15: Hemispheric directivity of broadband noise OASPL (0.1-13 kHz) of the UAM eVTOL quadrotor with three blades and the tip speed of 700 ft/s: (a) straight blade, (b) serrated blade, and (c) noise reduction.

CONCLUSIONS

This paper presented a state-of-the-art approach to predict broadband noise on rotors with serrated trailing edges. The original Lyu and Ayton's serrated airfoil section model, based on the Wiener-Hopf solution, was extended in this paper to include the finite span, the modified scattering coefficient, and the spanwise observer distance. These extensions were verified with Amiet's model and validated for serrated trailing-edge noise of a wing section, a hovering rotor, and a forward rotor. The effects of serration parameters on rotor broadband noise were studied. The broadband noise directivity of a serrated-blade quadrotor is investigated. The potential noise reduction using serrated trailing edges on an eVTOL quadrotor was analyzed. Important findings are summarized as follows:

- The serration height to wavelength ratio of 2 is a desirable selection to reduce rotor broadband noise, since further increasing the ratio only has slight noise reduction benefits. The preferred radial range to install trailing-edge serrations on a rotor blade is 50% to the tip, where the noise reduction increases linearly with the spanwise serrations added. However, adding serrations on the inboard 50% of the rotor blade only gives minimal noise reductions. The sine-wave, chopped peak, and saw-tooth serration shapes provide the largest noise reductions, and the square shape provides the least noise reduction among the studied shapes. A linearly decreasing serration height from the root to the tip slightly decreases the noise reduction compared to a constant height.
- On an eVTOL quadrotor, more than 9 dB noise reduction was found with serrated trailing edges. Higher noise reductions are observed on the serrated quadrotors with higher tip speeds and fewer blades.
- The serrated-blade UAM eVTOL quadrotor have the dipole broadband noise directivity, and noise reductions are observed at all observer angles with a primary noise reduction toward downward direction.

Although this research is focused on analytic and low-fidelity predictions of serrated trailing-edge noise, the results provide insights into important serration parameters in the context of rotor broadband noise and the significant potential to reduce UAM aircraft noise. It is suggested in the future study that the serration parameters or geometries are optimized to maximize the noise reduction and the predictions are further validated against experimental data or high-fidelity computational fluid dynamics (CFD) predictions. Finally, we note that the analytic model only considered the destructive interferences and it did not account for the acoustic source change due to the add-on serrations. This assumption and limitation can be revisited with more fundamental aeroacoustic research development.

REFERENCES

[1] Federal Aviation Administration, "Stage 3 Helicopter Noise Certification Standards," 14 CFR Part 36, September 18, 2012.

[2] Hasan, S., "Urban Air Mobility (UAM) Market Study," NASA Report HQ-E-DAA-TN63497s, NASA Headquarters, Washington, DC, November 1, 2018.

[3] Holden, J., and Goel, N., "Fast-Forwarding to a Future of On-Demand Urban Air Transportation," *White Paper, Uber*, 2016.

[4] Bain, J., Mikic, G., and Stoll, A., "Aerodynamic And Acoustic Design Of The Joby Aviation eVTOL Propeller," Vertical Flight Society 77th Annual Forum, Virtual Event, May 11-13, 2021.

[5] Huff, D. L., Henderson, B. S., Cluts, J. D., Boyle, D. K., Bennett, J., and Janzen, J., "Noise Measurements from Ground Tests of the Moog SureFly Vehicle," 2021 AIAA Aviation Forum, Virtual Event, August 2-6, 2021.

[6] Lee, S., Brentner, K., and Morris, P., "Long-Range and Nonlinear Propagation of Helicopter High-Speed Impulsive Noise," *Journal of the American Helicopter Society*, Vol. 62 (2), 2017, pp. 1–10.

[7] Jia, Z., Lee, S., Sharma, K., and Brentner, K., "Aeroacoustic Analysis of a Lift-Offset Coaxial Rotor Using High-Fidelity CFD/CSD Loose Coupling Simulation," *Journal of the American Helicopter Society*, Vol. 65 (1), 2020, pp. 1–15.

[8] Brooks, T., and Burley, C., "Blade Wake Interaction Noise for a Main Rotor," *Journal of the American Helicopter Society*, Vol. 49 (1), 2004, pp. 11–27.

[9] Brooks, T., Pope, D., and Marcolini, M., "Airfoil Self-noise and Prediction," , 1989. NASA RP 1218.

[10] Brooks, T., Marcolini, M., and Pope, D., "Main Rotor Broadband Noise Study in the DNW," *Journal of the American Helicopter Society*, Vol. 34 (2), 1989, pp. 3–12.

[11] Page, J., "In Situ Development and Application of Fly Neighborly Noise Abatement Procedures for Helicopters," Vertical Flight Society 75th Annual Forum, Philadelphia, Pennsylvania, May 13–16, 2019.

[12] Greenwood, E., "Dynamic Replanning of Low Noise Rotorcraft Operations," Vertical Flight Society 75th Annual Forum, Philadelphia, Pennsylvania, May 13–16, 2019.

[13] Krishnamurthy, S., Aumann, A. R., and Rizzi, S. A., "A Synthesis Plugin for Auralization of Rotor Self Noise," 2021 AIAA Aviation Forum, Virtual Event, August 2-6, 2021.

[14] Johnson, W., "A Quiet Helicopter for Air Taxi Operations," Proceedings of the 2020 VFS Aeromechanics for Advanced Vertical Flight Technical Meeting, San Jose, CA, January 21-23, 2020.

[15] Li, S., and Lee, S., "Acoustics Analysis of a Quiet Helicopter for Air Taxi Operations," Vertical Flight Society 77th Annual Forum, Virtual Event, May 11-13, 2021.

[16] Silva, C., and Johnson, W., "Practical Conceptual Design of Quieter Urban VTOL Aircraft," Vertical Flight Society 77th Annual Forum, Virtual Event, May 11-13, 2021.

[17]Currier, J. M., Hardesty, M., and O'Connell, J. M., "NOTAR system - A quiet character," AHS International Specialists' Meeting on Rotorcraft Basic Research, Philadelphia, PA, October 1991.

[18]Yu, Y., "Rotor Blade-Vortex Interaction Noise," *Progress in Aerospace Sciences*, Vol. 36, 2000, pp. 97–115.

[19]JanakiRam, R., Sim, B., Kitaplioglu, C., and Straub, F., "Blade-Vortex Interaction Noise Characteristics of a Full-Scale Active Flap Rotor," Proceedings of the American Helicopter Society 65th Annual Forum, Grapevine, Texas, May 27-29, 2009.

[20]Lee, S., Ayton, L., Bertagnolio, F., Moreau, S., Chong, T. P., and Joseph, P., "Turbulent boundary layer trailing-edge noise: Theory, computation, experiment, and application," *Progress in Aerospace Sciences*, Vol. 126, 2021, p. 100737.

[21]Szoke, M., and Azarpeyvand, M., "Active Flow Control Methods for the Reduction of Trailing Edge Noise," 23rd AIAA/CEAS Aeroacoustics Conference, Denver, Colorado, June 5-9, 2017.

[22]Shi, Y., and Lee, S., "Numerical Study of 3-D Finlets Using RANS CFD for Trailing Edge Noise Reduction," *International Journal of Aeroacoustics*, Vol. 19 (1-2), 2020, pp. 95–118.

[23]Ali, S. A. S., Szoke, M., Azarpeyvand, M., and da Silva, C. R. I., "Turbulent Flow Interaction with Porous Surfaces," 2018 AIAA/CEAS Aeroacoustics Conference, Atlanta, Georgia, June 25-29, 2018.

[24]Moreau, S., Dignou, B., Jaiswal, P., Yakhina, G. R., Pasco, Y., Sanjose, M., Alstrom, B., and Atalla, N., "Trailing-Edge Noise of a Flat Plate with Several Liner-Type Porous Appendices," 2018 AIAA/CEAS Aeroacoustics Conference, Atlanta, Georgia, June 25-29, 2018.

[25]Ayton, L. J., "Analytic Solution for Aerodynamic Noise Generated by Plates with Spanwise-Varying Trailing Edges," *Journal of Fluid Mechanics*, Vol. 849, 2018, p. 448–466.

[26]Ning, Z., Wlezien, R. W., and Hu, H., "An Experimental Study on Small UAV Propellers with Serrated Trailing Edges," 2017 AIAA AVIATION Forum, Denver, Colorado, 5-9 June, 2017.

[27]Oerlemans, S., Fisher, M., Maeder, T., and Kögler, K., "Reduction of Wind Turbine Noise Using Optimized Airfoils and Trailing-Edge Serrations," *AIAA Journal*, Vol. 47 (6), 2009, pp. 1470–1481.

[28]Cambray, A., Pang, E., Rezgui, D., Azarpeyvand, M., and Ali, S. A. S., "Investigation Towards a Better Understanding of Noise Generation from UAV Propellers," 2018 AIAA AVIATION Forum, Atlanta, Georgia, June 25-29, 2018.

[29]Yang, Y., Wang, Y., Liu, Y., Hu, H., and Li, Z., "Noise Reduction and Aerodynamics of Isolated Multi-Copter Rotors with Serrated Trailing Edges During Forward Flight," *Journal of Sound and Vibration*, Vol. 489, 2020, p. 115688.

[30]Howe, M., "Noise produced by a sawtooth trailing edge," *The Journal of the Acoustical Society of America*, Vol. 90 (1), 1991, pp. 482–487.

[31]Lyu, B., Azarpeyvand, M., and Sinayoko, S., "Prediction of noise from serrated trailing edges," *Journal of Fluid Mechanics*, Vol. 793, 2016, p. 556–588.

[32]Landahl, M., *Unsteady Transonic Flows*, Pergamon Press, 1961.

[33]Noble, B., *Methods Based on the Wiener–Hopf Technique for the Solution of Partial Differential Equations*, Pergamon Press, 1958.

[34]Huang, X., "Theoretical model of acoustic scattering from a flat plate with serrations," *Journal of Fluid Mechanics*, Vol. 819, 2017, p. 228–257.

[35]Lyu, B., and Ayton, L. J., "Rapid noise prediction models for serrated leading and trailing edges," *Journal of Sound and Vibration*, Vol. 469, 2020, p. 115136.

[36]Lee, S., "Empirical Wall-Pressure Spectral Modeling for Zero and Adverse Pressure Gradient Flows," *AIAA Journal*, Vol. 56 (5), 2018, pp. 1818–1829.

[37]Jones, L. E., and Sandberg, R. D., "Acoustic and hydrodynamic analysis of the flow around an aerofoil with trailing-edge serrations," *Journal of Fluid Mechanics*, Vol. 706, 2012, p. 295–322.

[38]Sanjosé, M., Moreau, S., Lyu, B., and Ayton, L. J., "Analytical, Numerical and Experimental Investigation of Trailing-Edge Noise Reduction on a Controlled Diffusion Airfoil with Serrations," 25th AIAA/CEAS Aeroacoustics Conference, Delft, The Netherlands, 20-23 May, 2019.

[39]Drela, M., *XFOIL: An Analysis and Design System for Low Reynolds Number Airfoils*, Vol. 54, Springer, 1989. Mueller T.J. (eds) Low Reynolds Number Aerodynamics.

[40]Peters, D., Boyd, D., and He, C., "Finite-State Induced-Flow Model for Rotors in Hover and Forward Flight," *Journal of the American Helicopter Society*, Vol. 34 (5), 1989, pp. 5–17.

[41]Johnson, W., *Helicopter Theory*, Dover Publication, 1994.

[42]Li, S., and Lee, S., "Prediction of Urban Air Mobility Multirotor VTOL Broadband Noise Using UCD-QuietFly," *Journal of the American Helicopter Society*, Vol. 66 (3), 2021, pp. 1–13.

[43]Amiet, R., "Noise Due to Turbulent Flow Past a Trailing Edge," *Journal of Sound and Vibration*, Vol. 47 (3), 1976, pp. 387–393.

[44]Li, S., and Lee, S., "Prediction of Rotorcraft Broadband Trailing-Edge Noise and Parameter Sensitivity Study," *Journal of the American Helicopter Society*, Vol. 65 (4), 2020, pp. 1–14.

[45]Lighthill, M., "On Sound Generated Aerodynamically I. General Theory," *Proceedings of the Royal Society*, Vol. A211, 1952, pp. 564–587.

[46]Roger, M., and Moreau, S., "Back-Scattering Correction and Further Extensions of Amiet's Trailing-Edge Noise Model. Part 1: Theory," *Journal of Sound and Vibration*, Vol. 286, 2005, pp. 477 – 506.

[47]Corcos, G. M., "The structure of the turbulent pressure field in boundary-layer flows," *Journal of Fluid Mechanics*, Vol. 18 (3), 1964, p. 353–378.

[48]Li, S., and Lee, S., "Predictions and Validations of Small-Scale Rotor Noise Using UCD-QuietFly," Proceedings of the American Helicopter Society Technical Conference on Aeromechanics Design for Transformative Vertical Flight, San Jose, CA, January 25-27, 2022.

[49]Kholodov, P., and Moreau, S., "Optimization of trailing-edge serrations with and without slits for broadband noise reduction," *Journal of Sound Vibration*, Vol. 490, 2021, p. 115736.

[50]Li, S., "Development of Rotorcraft Forward Flight Analysis Code Using the Finite-State Dynamic Inflow Model," Master's thesis, University of California Davis, August 2020.

[51]Li, S., and Lee, S., "Acoustic Analysis and Sound Quality Assessment of a Quiet Helicopter for Air Taxi Operations," *Journal of the American Helicopter Society*, Vol. 67 (3), 2022, pp. 1–15.

[52]Li, S., and Lee, S., "A Machine Learning-Based Fast Prediction of Rotorcraft Broadband Noise," Proceedings of the 2020 AIAA Aviation Forum, Virtual Event, June 15-19, 2020.

[53]Leon, C., Ragni, D., Probsting, S., Scarano, F., and Madsen, J., "Flow Topology and Acoustic Emissions of Trailing Edge Serrations at Incidence," *Experiments in Fluids*, Vol. 57 (91), 2016, pp. 1–17.

[54]Chong, T. P., and Vathylakis, A., "On the aeroacoustic and flow structures developed on a flat plate with a serrated sawtooth trailing edge," *Journal of Sound and Vibration*, Vol. 354, 2015, pp. 65–90.

[55]Begault, D., "Ambient Noise Measurement for UAM Metric Analysis and Research," Acoustics and Urban Air Mobility Technical Working Group Meeting, Hampton, VA, April 09-11, 2019.

[56]Sanjose, M., Meon, C., Moreau, S., Idier, A., and Laffay, P., "Direct Numerical Simulation of Acoustic Reduction Using Serrated Trailing-Edge on an Ssolated Airfoil," 20th AIAA/CEAS Aeroacoustics Conference, Atlanta, GA, June 16-20, 2014.